Hierarchical Templating of a $BiFeO_3$–$CoFe_2O_4$ Multiferroic Nanocomposite by a Triblock Terpolymer Film

Hong Kyoon Choi,[†] Nicolas M. Aimon,[†] Dong Hun Kim,[†] Xue Yin Sun,[†,‡] Jessica Gwyther,[§] Ian Manners,[§] and Caroline A. Ross*[,†]

[†]Department of Materials Science and Engineering, Massachusetts Institute of Technology, Cambridge, Massachusetts 02139, United States, [‡]School of Materials Science and Engineering, Harbin Institute of Technology, Harbin 150001, People's Republic of China, and [§]School of Chemistry, University of Bristol, Bristol BS8 1TS U.K.

ABSTRACT A process route to fabricate templated $BiFeO_3/CoFe_2O_4$ (BFO/CFO) vertical nanocomposites is presented in which the self-assembly of the BFO/CFO is guided using a self-assembled triblock terpolymer. A linear triblock terpolymer was selected instead of a diblock copolymer in order to produce a square-symmetry template, which had a period of 44 nm. The triblock terpolymer pattern was transferred to a (001) $Nb:SrTiO_3$ substrate to produce pits that formed preferential sites for the nucleation of CFO crystals, in contrast to the BFO, which wetted the flat regions of the substrate. The crystallographic orientation and magnetic properties of the templated BFO/CFO were characterized.

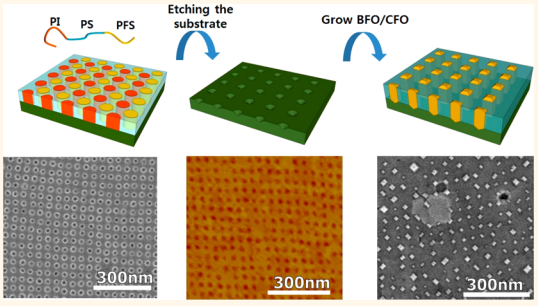

KEYWORDS: directed self-assembly · spinel-perovskite nanocomposite · triblock terpolymer

In a vertically aligned nanocomposite oxide thin film, two co-deposited, immiscible oxide phases grow epitaxially on a single crystal substrate to form a two-phase columnar structure such as a checkerboard, a labyrinth, or pillars of one phase embedded in a matrix of the other phase. Oxide nanocomposite films can show multifunctionality arising from the properties and geometries of the phases, and strain-mediated coupling between the two phases can lead to magnetoelectric behavior when one phase is ferroelectric and the other ferromagnetic.[1−6] Among the variety of nanocomposite thin films studied, $BiFeO_3/CoFe_2O_4$ (BFO/CFO) grown on (001) $SrTiO_3$ (STO) substrate is the most thoroughly explored system[7−14] owing to its well-defined self-assembled columnar nanostructure consisting of magnetic CFO pillars in a ferroelectric BFO matrix. Strong magnetoelectric coupling behavior has been demonstrated in which switching of magnetization in the CFO pillars was controlled by the electric field.[11,12] This coupling provides a basis for proposed magnetic memory or logic devices.[15]

In order to use multiferroic columnar nanostructures in device applications, it is necessary to control the location of the pillars on the substrate. To date, three methods have been demonstrated for templating the CFO pillar locations. Comes *et al.* made square arrays of CFO pillars with a 100−200 nm period in a BFO matrix by patterning a thin CFO film to form CFO seeds using electron beam lithography (EBL) and ion milling.[16] Stratulat *et al.* used a lift-off process with hard masks made from EBL-patterned gold or from anodic aluminum oxide (AAO) to create CFO nuclei with a 200−300 nm period.[17] Recently, we presented an approach that takes advantage of the change in surface energy between CFO and different crystal orientations of the substrate.[18] A focused ion beam (FIB) was used to make pits in the STO substrate of pitch 60−100 nm in which CFO nuclei selectively formed.[18,19] While these approaches achieved well-ordered BFO/CFO

* Address correspondence to caross@mit.edu.

Received for review June 7, 2014 and accepted September 3, 2014.

Published online September 03, 2014
10.1021/nn503100s

nanocomposites, the serial nature of EBL and FIB restricts them to small-area fabrication, while the self-assembled AAO template can cover larger areas, but it is limited to producing a hexagonal close-packed array.

Self-assembled block copolymer thin films offer a next-generation nanolithography method that could overcome the cost and resolution challenges facing current UV photolithography technology.[20−29] Diblock copolymers produce thin film patterns consisting of lines or close-packed dots or holes, but thin films of a linear triblock terpolymer can instead produce square-packed arrangements of dots or holes.[30−34] In this work, we demonstrate the templating of a square-symmetry BFO/CFO nanocomposite with a period of 44 nm using a linear triblock terpolymer film as a template for topographically patterning a substrate. Compared to previously reported templating methods,[16−18] a patterning process based on a block copolymer can provide a much smaller periodicity array over a large area with a short process time. Moreover, the block copolymer can be templated using for example topographical trenches to impose long-range order on the pattern.[35,36]

RESULTS AND DISCUSSION

A schematic of the overall experimental process is described in Figure 1, and details are given in the Methods section. First, a polyisoprene-*b*-polystyrene-*b*-polyferrocenylsilane (PI-*b*-PS-*b*-PFS, M_n = 82 kg/mol, $f_{PI} = 0.25$, $f_{PS} = 0.65$, $f_{PFS} = 0.10$)/PS homopolymer blend (ISF/hS) was spin coated on a single crystal (001) Nb-doped $SrTiO_3$ (Nb:STO) substrate on which a poly-(2-vinylpyridine) (P2VP) brush was grafted to promote out-of-plane orientation of the microdomains.[37] The spin-coated thin film was then solvent-annealed in chloroform vapor using a continuous flow system in which the vapor pressure of solvent is controlled by changing the flow rate of saturated solvent vapor and nitrogen gas.[38] The annealed thin film morphology of the ISF/hS blend is shown schematically in Figure 1i. A square symmetry array of alternating PI and PFS cylinders was formed in a PS matrix. The addition of homo-PS to the triblock terpolymer stabilized the square symmetry by relaxing the highly stretched triblock terpolymer chains.[34]

Immersing the self-assembled thin film in hexane, a selective solvent for PI, promoted the diffusion of PI to the top surface of the film, and rapid quenching of the swelled film generated a square array of holes at the original locations of the PI cylinders by distributing the PI on the film surface (Figure 1ii).[39,40] Figure 2a shows a SEM image of the ISF/hS thin film morphology after surface reconstruction in hexane. The periodicity and the average diameter of the holes were 44 and 15 nm, respectively. The residual polymer at the bottom of the holes was then removed by a short O_2 reactive ion etch (RIE). In this step, the diameter of the holes can be easily tuned by changing the RIE time as shown in Figure 2b and c, where the average diameter of the holes was 20 and 29 nm after 5 and 15 s of O_2 RIE, respectively.

The porous polymer film was used as a mask to pattern pits into the underlying Nb:STO substrate (Figure 1iii) by wet etching in aqua regia for 20 min followed by air calcination at 600 °C to remove residual polymer (Figure 1iv).[41] Figure 2d and e are AFM height images of surface-patterned Nb:STO substrates templated from a polymer film shown in Figure 2b and c, respectively. The diameters of the pits were consistent with the size of the holes in the polymer masks, and the depth of the pits in both cases was 2.5 nm.

CFO nuclei were then grown by depositing a small amount of CFO on patterned Nb:STO. A thin CFO layer forms islands on flat (001) Nb:STO even without BFO co-deposition;[18] that is, the wettability of CFO is very

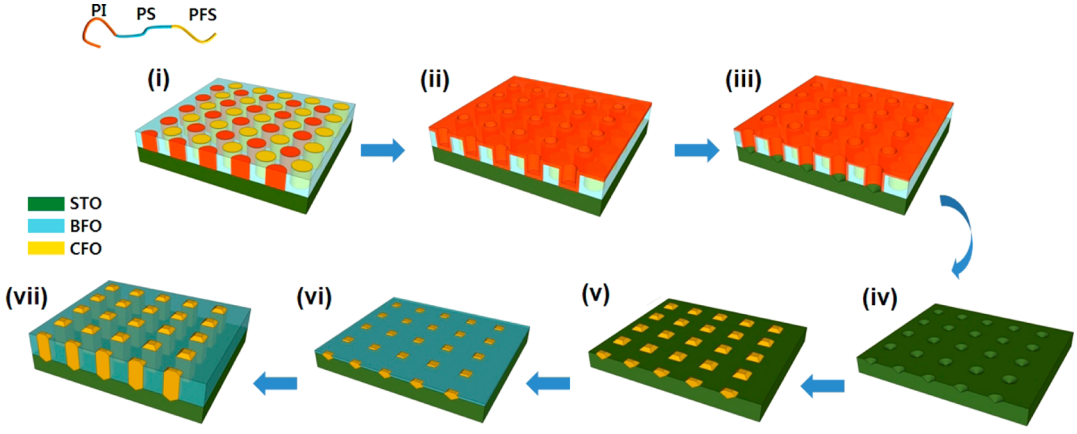

Figure 1. Schematic illustration of the fabrication process of a templated BFO/CFO nanocomposite. (i) Self-assembled square-symmetry microdomain array from PI-*b*-PS-*b*-PFS/PS blend. (ii) Square array of holes was generated from PI microdomains via surface reconstruction in hexane. (iii) Residual polymer layer on the bottom of holes was removed by a short O_2 plasma, then the STO substrate was etched through the polymer mask by immersing in aqua regia. (iv) Square array of pits in the STO surface was revealed after removing the polymer template. (v) CFO nuclei were selectively grown in patterned pits. (vi) A thin BFO layer was deposited to cover the mesas. (vii) A thick BFO/CFO nanocomposite was deposited, guided by the thin BFO/CFO composite.

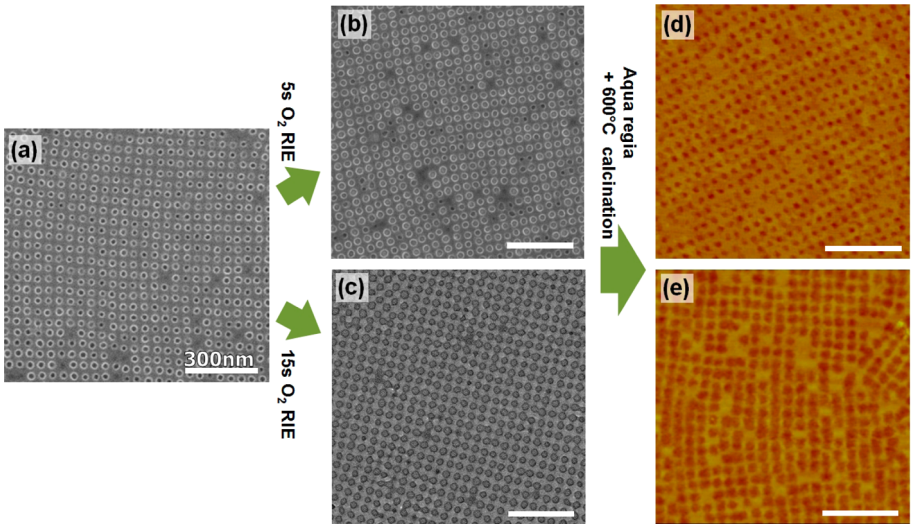

Figure 2. SEM images of PI-*b*-PS-*b*-PFS/PS blend thin film (a) after surface reconstruction, (b) after O_2 RIE for 5 s, and (c) after O_2 RIE for 15 s. AFM height images of surface-patterned Nb:STO (d) etched using the polymer mask shown in (b) and (e) etched using the polymer mask shown in (c). All scale bars are 300 nm.

low[7] on the (001) facet of the substrate. However, the etched pits are bounded by other facets and provide preferential nucleation sites for CFO (Figure 1v). As a result, a square array of CFO nuclei was formed correlated with the surface topographic pattern of the substrate. Thermal annealing in the pulsed laser deposition (PLD) chamber at 680 °C was carried out after CFO deposition to promote {111} faceting of the CFO nuclei. Figure 3a shows CFO nuclei grown on the patterned Nb:STO substrate shown in Figure 2d. CFO nuclei are present in the pits, but there were still tiny nuclei on the mesas, and some of the CFO nuclei in pits did not show distinct facets.

A thin BFO layer was then deposited to cover the unetched area of the substrate and to prevent formation of additional CFO nuclei between the pits (Figure 1vi). Figure 3b shows the CFO nuclei with an approximately 4 nm thick BFO layer, which covered the small CFO nuclei present on the mesa. If the BFO passivation layer was thicker than the CFO nuclei height, the excess BFO formed ridges around the CFO nuclei, as shown in Figure S1a in the Supporting Information. CFO nucleation on pits with a larger diameter was also examined. Figure S1b shows CFO nuclei grown on the substrate shown in Figure 2e. There was insufficient CFO to fill the pits, and CFO nuclei formed mostly at the edges of pits, with more than one nucleus in each pit.[19]

Finally, a thick layer of the BFO/CFO composite was deposited by alternating ablation[13] from the CFO and BFO targets (Figure 1vii). Deposition from two targets allows for a range of average film compositions rather than obtaining a fixed composition from a target containing both components of the nanocomposite. Moreover, the deposition conditions for each component can be separately adjusted. In our sample preparation process a lower laser frequency (5 Hz) was used for CFO deposition to allow enough diffusion for adatoms to reach the nucleation sites, while a higher laser frequency (20 Hz) was used for BFO deposition to prevent coarsening. Figure 3c shows a thick (~40 nm) templated BFO/CFO nanocomposite. The CFO seed layer, CFO anneal, BFO layer, and nanocomposite depositions took place sequentially without breaking the vacuum. The pillar diameter is governed by the relative fluxes of CFO and BFO and does not depend on the pit diameter unless the pits are so large that multiple nuclei form in each one (Figure S1b).

Figure 3d shows a tilted SEM image of free-standing CFO pillars after selectively etching the BFO matrix in 5% HCl aqueous solution.[8] This reveals that CFO pillars grew vertically throughout the film. However, some short CFO pillars also were observed, as indicated by a red circle in Figure 3d, that did not grow up to the top surface and were overgrown with BFO, producing vacant sites in the top view of the composite. These pillars overgrown by BFO may have originated from smaller CFO nuclei (shown by a red circle in Figure 3b) formed in the smaller and shallower pits. A cross sectional TEM analysis of the templated BFO/CFO composite was also conducted. Figure 3e shows the vertical interface between the BFO matrix and CFO pillars and well-defined (111) and (001) facets of CFO protruding from the top surface of the BFO, as seen in several previous observations of BFO/CFO nanocomposites.[7,9] It is also evident that CFO pillars formed at the locations of the pits as indicated with a dotted line in Figure 3e. The high-resolution TEM image in the inset of Figure 3e shows the lattice fringes and confirmed that both BFO and CFO phases were epitaxial single crystals.

We next compare the CFO pillar to pillar distance distribution between templated and untemplated BFO/

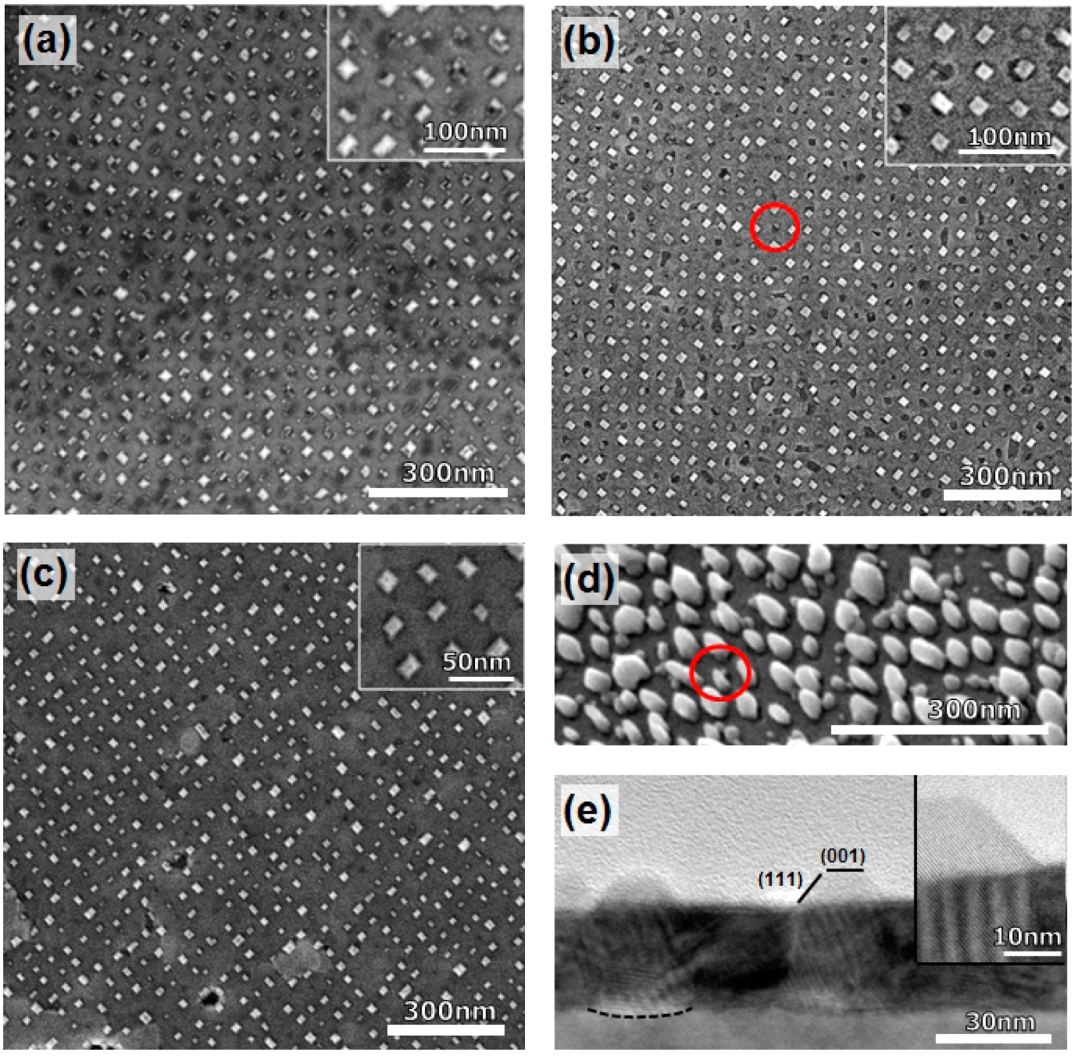

Figure 3. SEM images of (a) CFO nuclei grown on etched Nb:STO, (b) thin layer of BFO/CFO nanocomposite after depositing BFO, and (c) thick BFO/CFO nanocomposite. (d) Tilted view SEM image of free-standing CFO pillars after selectively removing the BFO matrix from the BFO/CFO nanocomposite. (e) TEM cross-sectional image of the templated BFO/CFO nanocomposite. TEM image was taken along the (110) zone axis. The dashed line indicates the outline of a pit. Red circles in (b) and (d) indicate a smaller CFO nucleus and a short CFO pillar, respectively.

CFO nanocomposites grown under the same PLD conditions. The SEM images used for image analysis are shown in Figure S2a and b. The pillar to pillar distance was defined as the average distance from the center of one pillar to the center of its four nearest neighbors, with data collected from about 2300 CFO pillars from each sample. The distributions of pillar to pillar distance are plotted in Figure 4a. As expected, the pillar to pillar distance in templated BFO/CFO nanocomposites had a narrow distribution, and most pillar to pillar distances were between 40 and 55 nm, corresponding to the periodicity of the block copolymer used in this study. On the other hand, CFO pillars in untemplated BFO/CFO nanocomposites were less dense, and pillar to pillar distances were broadly distributed between 35 and 100 nm. This shows that templating can select a periodicity within the range of natural periodicities possible in the system.[42]

Finally, magnetic hysteresis loops of the templated BFO/CFO nanocomposite were measured at room temperature by vibrating sample magnetometer (VSM), as shown in Figure 3b. The magnetization values were normalized by the volume of the film. The measured saturation magnetization was about 85 emu cm^{-3}, which is about 20% of the bulk saturation magnetization of CFO (400 emu cm^{-3}).[13] This is reasonable considering the volume fraction of CFO in the BFO/CFO nanocomposites.

The templated BFO/CFO nanocomposite showed out-of-plane magnetic anisotropy as typically seen in nanocomposites grown on (001) STO. This out-of-plane magnetic anisotropy is attributed to a combination of the shape anisotropy of CFO pillars and a magnetoelastic anisotropy due to the out-of-plane compression of the CFO caused by lattice mismatch with the BFO phase.[13,43] The compressive strain of the CFO phase in the out-of-plane direction was found from the position

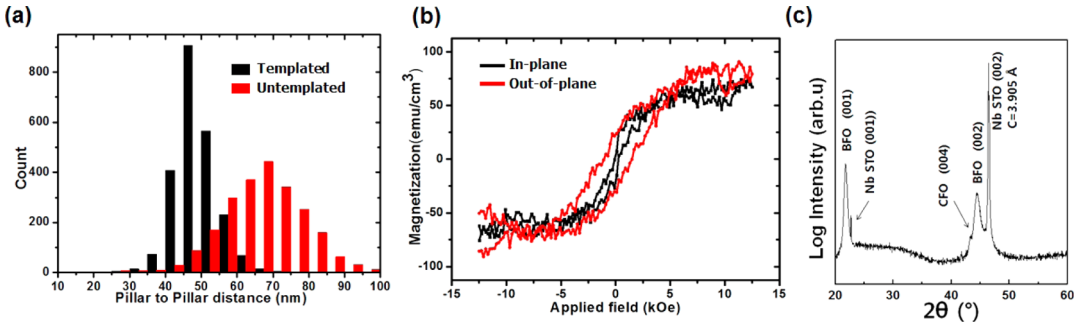

Figure 4. (a) Distributions of pillar to pillar distances of templated (black) and untemplated (red) BFO/CFO nanocomposites. The SEM images used in this analysis are shown in Figure S2. (b) In-plane and out-of-plane magnetization hysteresis loops of templated BFO/CFO nanocomposite measured at room temperature by VSM. (c) XRD pattern of templated sample.

of the CFO (004) peak shown in Figure 3c. The X-ray diffractometer (XRD) data of Figure 3c also confirm the epitaxial growth of the two phases on the substrate. The out-of-plane lattice parameter of the CFO phase was $a_{CFO} = 8.363 \pm 0.004$ Å, corresponding to a compressive strain $\varepsilon = -0.20 \pm 0.05\%$. This strain, calculated with respect to the bulk value ($a_{CFO} = 8.380$ Å),[13,44] is similar to that obtained in an untemplated BFO/CFO nanocomposite grown under similar deposition conditions.[13]

The measured strain would suggest a magnetoelastic anisotropy field $H_{k,me} \approx 7$ kOe, in addition to the shape anisotropy contribution (which would be $H_{k,s} = 1.9$ kOe for a rod-shaped pillar of aspect ratio 3:1 and less for lower aspect ratios). The measured total anisotropy field from extrapolation of the hard axis (in-plane) loop to saturation was ~4 kOe, which is lower than $H_{k,s} + H_{k,me}$ but which nevertheless suggests that magnetoelastic anisotropy provides a major contribution to the total anisotropy. The discrepancy between estimated and measured anisotropy fields could have various origins, such as a nonbulk magnetostriction value, an in-plane strain or an inhomogeneous strain state.[14]

CONCLUSIONS

A templated square array of CFO pillars in BFO was fabricated using a self-assembled linear triblock terpolymer as an etch mask to pattern the substrate. By taking advantage of the different wetting behavior of perovskite and spinel phases, the BFO/CFO nanocolumnar structure was guided by the surface topography of the Nb:STO substrate. Compared to previously reported templating methods, this approach achieved the smallest periodicity, 44 nm, and also has the advantage of patterning large areas with low cost and a short process time. The pillar density demonstrated in this study was 5×10^{10} cm^{-2} and could be further increased by using a lower molecular weight triblock terpolymer. The triblock terpolymer patterns had good short-range order however, long-range order, or aperiodic arrangements, can be accomplished using directed self-assembly guided by a sparse substrate pattern.[37] The crystallographic orientation and magnetic anisotropy of the templated sample were similar to those of an untemplated composite described in a prior study.[13] The magnetoelectric coupling behavior of templated BFO/CFO nanocomposites of period 67 nm and above measured using scanning probe microscopy is described elsewhere.[45] This hierarchical process in which one self-assembling system templates another could facilitate the incorporation of multiferroic nanocomposites into magnetic memory or logic devices.

EXPERIMENTAL METHODS

Block Copolymer Self-Assembly and Pattern Transfer. (001)-oriented Nb-doped STO substrates (0.7% Nb, MTI Corporation) were used. For the brush layer, a P2VP ($M_n = 6.2$ kg/mol, Polymer Source Inc.) solution was spin-coated on the Nb:STO substrate and annealed at 170 °C overnight under vacuum. The ungrafted polymer was then removed by rinsing with toluene. The synthesis processes of PI-*b*-PS-*b*-PFS, $M_n = 82$ kg/mol, $f_{PI} = 0.25$, $f_{PS} = 0.65$, $f_{PFS} = 0.10$, are described in ref 34. The blend solution of the PI-*b*-PS-*b*-PFS and PS homopolymer ($M_n = 27$ kg/mol, Polymer Source Inc.) at a weight ratio of 0.85:0.15 was spin coated on a substrate with a thickness of 32 nm from toluene. The spin-coated thin polymer film was then solvent annealed in a flow-controlled solvent annealing system where saturated chloroform vapor and pure nitrogen gas are continuously flowed into the annealing chamber.[38] The triblock terpolymer films were annealed for 1 h in an atmosphere resulting from an 8:2 ratio of saturated chloroform vapor and pure nitrogen gas; that is, the chloroform partial pressure was estimated to be 205 Torr at room temperature.

To open the holes in the self-assembled ISF/hS film, the film was immersed in hexane for 20 s and quenched immediately using a nitrogen gun. Then 5 s of oxygen RIE (10 mTorr, 90 W, Plasma Therm 790) was applied to remove the polymer layer at the bottom of the holes and also slightly widen the holes. The Nb:STO substrate was then etched through the polymer holes in aqua regia (a mixture of concentrated HCl and HNO_3 at a volume ratio of 3:1) for 20 min followed by air calcination at 600 °C to remove the residual polymer template, leaving a square array of pits in the Nb:STO substrate. The substrate was then cleaned by dipping in concentrated HCl for 30 s to remove residual Fe contained in the PFS phase.

BFO/CFO Film Deposition. BFO/CFO oxide films were grown by pulsed laser deposition using a KrF excimer laser (Coherent) at an operating wavelength of 248 nm. The BFO and CFO targets were purchased from Plasmaterials. The oxygen pressure in the chamber for all processes was 5 mTorr. A CFO nucleation layer was grown on patterned Nb:STO at 640 °C with a laser fluence of 2 J/cm^2 and a repetition rate of 1 Hz. The CFO nucleation layer was then annealed in the chamber at 680 °C and 5 mTorr oxygen pressure for 12 h. A thin BFO layer was deposited at a lower temperature of 580 °C with a higher laser fluence of 2.6 J/cm^2 and a higher repetition rate of 20 Hz. The thick BFO/CFO composite was grown by alternately depositing a submonolayer thickness of BFO and CFO. The temperature, fluence, and repetition rate were 580 °C, 2.6 J/cm^2, and 20 Hz (for BFO) or 5 Hz (for CFO), respectively. The detailed deposition methods are described elsewhere.[13]

Characterization. A Helios Nanolab 600 microscope was used for SEM imaging and TEM sample preparation. The cross sectional TEM analysis was conducted using a JEOL 2010F field emission TEM. The magnetic properties of composite films were measured using VSM (ADE model 1660) at room temperature, and the background signal from the substrate and holder was excluded. The magnetization values were normalized by the net volume of the film instead of the volume of CFO. Structure and phase formation of films were investigated by X-ray diffractometer (PANalytical X'Pert Pro). The image analysis to obtain pillar to pillar distances was conducted using ImageJ software.[46]

Conflict of Interest: The authors declare no competing financial interest.

Acknowledgment. Support from NSF award DMR1007760, EPSRC, and from FAME, one of six centers of STARnet, an SRC program sponsored by MARCO and DARPA, is gratefully acknowledged. Shared facilities of CMSE award NSF DMR 0819762 were used.

Supporting Information Available: SEM images of CFO nuclei and a thin layer of BFO/CFO nanocomposite grown in different conditions and large-area SEM images of templated/untemplated BFO/CFO nanocomposite. This material is available free of charge *via* the Internet at http://pubs.acs.org.

REFERENCES AND NOTES

1. MacManus-Driscoll, J. L. Self-Assembled Heteroepitaxial Oxide Nanocomposite Thin Film Structures: Designing Interface-Induced Functionality in Electronic Materials. *Adv. Funct. Mater.* **2010**, *20*, 2035–2045.
2. Zheng, H.; Wang, J.; Lofland, S. E.; Ma, Z.; Mohaddes-Ardabili, L.; Zhao, T.; Salamanca-Riba, L.; Shinde, S. R.; Ogale, S. B.; Bai, F.; *et al*. Multiferroic $BaTiO_3$-$CoFe_2O_4$ Nanostructures. *Science* **2004**, *303*, 661–663.
3. Nan, C.-W.; Liu, G.; Lin, Y.; Chen, H. Magnetic-Field-Induced Electric Polarization in Multiferroic Nanostructures. *Phys. Rev. Lett.* **2005**, *94*, 197203.
4. Vaz, C. A. F.; Hoffman, J.; Ahn, C. H.; Ramesh, R. Magnetoelectric Coupling Effects in Multiferroic Complex Oxide Composite Structures. *Adv. Mater.* **2010**, *22*, 2900–2918.
5. Liu, B.; Sun, T.; He, J.; Dravid, V. P. Sol−Gel-Derived Epitaxial Nanocomposite Thin Films with Large Sharp Magnetoelectric Effect. *ACS Nano* **2010**, *4*, 6836–6842.
6. Alexe, M.; Hesse, D. Self-Assembled Nanoscale Ferroelectrics. *J. Mater. Sci.* **2006**, *41*, 1–11.
7. Zheng, H.; Straub, F.; Zhan, Q.; Yang, P.-L.; Hsieh, W.-K.; Zavaliche, F.; Chu, Y.-H.; Dahmen, U.; Ramesh, R. Self-Assembled Growth of $BiFeO_3$−$CoFe_2O_4$ Nanostructures. *Adv. Mater.* **2006**, *18*, 2747–2752.
8. Dix, N.; Muralidharan, R.; Guyonnet, J.; Warot-Fonrose, B.; Varela, M.; Paruch, P.; Sánchez, F.; Fontcuberta, J. On the Strain Coupling across Vertical Interfaces of Switchable $BiFeO_3$−$CoFe_2O_4$ Multiferroic Nanostructures. *Appl. Phys. Lett.* **2009**, *95*, 062907.
9. Zheng, H.; Zhan, Q.; Zavaliche, F.; Sherburne, M.; Straub, F.; Cruz, M. P.; Chen, L.-Q.; Dahmen, U.; Ramesh, R. Controlling Self-Assembled Perovskite-Spinel Nanostructures. *Nano Lett.* **2006**, *6*, 1401–1407.
10. Dix, N.; Muralidharan, R.; Rebled, J.-M.; Estradé, S.; Peiró, F.; Varela, M.; Fontcuberta, J.; Sánchez, F. Selectable Spontaneous Polarization Direction and Magnetic Anisotropy in $BiFeO_3$-$CoFe_2O_4$ Epitaxial Nanostructures. *ACS Nano* **2010**, *4*, 4955–4961.
11. Zavaliche, F.; Zheng, H.; Mohaddes-Ardabili, L.; Yang, S. Y.; Zhan, Q.; Shafer, P.; Reilly, E.; Chopdekar, R.; Jia, Y.; Wright, P.; *et al*. Electric Field-Induced Magnetization Switching in Epitaxial Columnar Nanostructures. *Nano Lett.* **2005**, *5*, 1793–1796.
12. Zavaliche, F.; Zhao, T.; Zheng, H.; Straub, F.; Cruz, M. P.; Yang, P.-L.; Hao, D.; Ramesh, R. Electrically Assisted Magnetic Recording in Multiferroic Nanostructures. *Nano Lett.* **2007**, *7*, 1586–1590.
13. Aimon, N. M.; Kim, D. H.; Choi, H. K.; Ross, C. A. Deposition of Epitaxial $BiFeO_3$/$CoFe_2O_4$ Nanocomposites on (001) $SrTiO_3$ by Combinatorial Pulsed Laser Deposition. *Appl. Phys. Lett.* **2012**, *100*, 092901.
14. Aimon, N. M.; Liao, J.; Ross, C. A. Simulation of Inhomogeneous Magnetoelastic Anisotropy in Ferroelectric/Ferromagnetic Nanocomposites. *Appl. Phys. Lett.* **2012**, *101*, 232901.
15. Wolf, S. A.; Lu, J.; Stan, M. R.; Chen, E.; Treger, D. M. The Promise of Nanomagnetics and Spintronics for Future Logic and Universal Memory. *Proc. IEEE* **2010**, *98*, 2155–2168.
16. Comes, R.; Liu, H.; Khokhlov, M.; Kasica, R.; Lu, J.; Wolf, S. A. Directed Self-Assembly of Epitaxial $CoFe_2O_4$-$BiFeO_3$ Multiferroic Nanocomposites. *Nano Lett.* **2012**, *12*, 2367–2373.
17. Stratulat, S. M.; Lu, X.; Morelli, A.; Hesse, D.; Erfurth, W.; Alexe, M. Nucleation-Induced Self-Assembly of Multiferroic $BiFeO_3$−$CoFe_2O_4$ Nanocomposites. *Nano Lett.* **2013**, *13*, 3884–3889.
18. Aimon, N. M.; Choi, H. K.; Sun, X. Y.; Kim, D. H.; Ross, C. A. Templated Self-Assembly of Functional Oxide Nanocomposites. *Adv. Mater.* **2014**, *26*, 3063–3067.
19. Du, Y.; Atha, S.; Hull, R.; Groves, J. F.; Lyubinetsky, I.; Baer, D. R. Focused-Ion-Beam Directed Self-Assembly of Cu_2O Islands on $SrTiO_3$(100). *Appl. Phys. Lett.* **2004**, *84*, 5213–5215.
20. Darling, S. B. Directing the Self-Assembly of Block Copolymers. *Prog. Polym. Sci.* **2007**, *32*, 1152–1204.
21. Segalman, R. A. Patterning with Block Copolymer Thin Films. *Mater. Sci. Eng., R* **2005**, *48*, 191–226.
22. Park, C.; Yoon, J.; Thomas, E. L. Enabling Nanotechnology with Self Assembled Block Copolymer Patterns. *Polymer* **2003**, *44*, 6725–6760.
23. Lazzari, M.; López-Quintela, M. A. Block Copolymers as a Tool for Nanomaterial Fabrication. *Adv. Mater.* **2003**, *15*, 1583.
24. Bang, B. J.; Jeong, U.; Ryu, D. Y.; Russell, T. P.; Hawker, C. J. Block Copolymer Nanolithography: Translation of Molecular Level Control to Nanoscale Patterns. *Adv. Mater.* **2009**, *21*, 4769–4792.
25. Cheng, J. Y.; Ross, C. A.; Smith, H. I.; Thomas, E. L. Templated Self-Assembly of Block Copolymers: Top-Down Helps Bottom-Up. *Adv. Mater.* **2006**, *18*, 2505–2521.
26. Nunns, A.; Gwyther, J.; Manners, I. Inorganic Block Copolymer Lithography. *Polymer* **2013**, *54*, 1269–1284.
27. Korczagin, I.; Lammertink, R. G. H.; Hempenius, M. A.; Golze, S.; Vancso, G. J. Surface Nano- and Microstructuring with Organometallic Polymers. *Adv. Polym. Sci.* **2006**, *200*, 91–117.
28. Han, W.; Byun, M.; Li, B.; Pang, X.; Lin, Z. A Simple Route to Hierarchically Assembled Micelles and Inorganic Nanoparticles. *Angew. Chem., Int. Ed.* **2012**, *51*, 12588–12592.
29. Bo, L.; Wei, H.; Beibei, J.; Zhiqun, L. Crafting Threads of Diblock. *ACS Nano* **2014**, *8*, 2936–2942.
30. Mogi, Y.; Kotsuji, H.; Kaneko, Y.; Mori, K.; Matsushita, Y.; Noda, I. Preparation and Morphology of Triblock Copolymers of the ABC Type. *Macromolecules* **1992**, *25*, 5408–5411.
31. Zheng, W.; Wang, Z.-G. Morphology of ABC Triblock Copolymers. *Macromolecules* **1995**, *28*, 7215–7223.

32. Mogi, Y.; Nomura, M.; Kotsuji, H.; Ohnishi, K.; Matsushita, Y.; Noda, I. Superlattice Structures in Morphologies of the ABC Triblock Copolymers. *Macromolecules* **1994**, *27*, 6755–6760.
33. Tang, C.; Bang, J.; Stein, G. E.; Fredrickson, G. H.; Hawker, C. J.; Kramer, E. J.; Sprung, M.; Wang, J. Square Packing and Structural Arrangement of ABC Triblock Copolymer Spheres in Thin Films. *Macromolecules* **2008**, *41*, 4328–4339.
34. Chuang, V. P.; Gwyther, J.; Mickiewicz, R. A.; Manners, I.; Ross, C. A. Templated Self-Assembly of Square Symmetry Arrays from an ABC Triblock Terpolymer. *Nano Lett.* **2009**, *9*, 4364–4369.
35. Sundrani, D.; Darling, S. B.; Sibener, S. J. Hierarchical Assembly and Compliance of Aligned Nanoscale Polymer Cylinders in Confinement. *Langmuir* **2004**, *20*, 5091–5099.
36. Jung, Y. S.; Ross, C. A. Orientation-Controlled Self-Assembled Nanolithography Using a Polystyrene-Polydimethylsiloxane Block Copolymer. *Nano Lett.* **2007**, *7*, 2046–2050.
37. Son, J. G.; Gwyther, J.; Chang, J.-B.; Berggren, K. K.; Manners, I.; Ross, C. A. Highly Ordered Square Arrays from a Templated ABC Triblock Terpolymer. *Nano Lett.* **2011**, *11*, 2849–2855.
38. Gotrik, K.; Hannon, A. F.; Son, J. G.; Keller, B.; Alexander-Katz, A.; Ross, C. A. Morphology Control in Block Copolymer Films Using Mixed Solvent Vapors. *ACS Nano* **2012**, *6*, 8052–8059.
39. Choi, H. K.; Gwyther, J.; Manners, I.; Ross, C. A. Square Arrays of Holes and Dots Patterned from a Linear ABC Triblock Terpolymer. *ACS Nano* **2012**, *6*, 8342–8348.
40. Xu, T.; Stevens, J.; Villa, J. A.; Goldbach, J. T.; Guarini, K. W.; Black, C. T.; Hawker, C. J.; Russell, T. P. Block Copolymer Surface Reconstuction: A Reversible Route to Nanoporous Films. *Adv. Funct. Mater.* **2003**, *13*, 698–702.
41. Doan, T.-D.; Giocondi, J. L.; Rohrer, G. S.; Salvador, P. A. Surface Engineering along the Close-Packed Direction of $SrTiO_3$. *J. Cryst. Growth* **2001**, *225*, 178–182.
42. Okada, K.; Sakamoto, T.; Fujiwara, K.; Hattori, A. N.; Kanki, T.; Tanaka, H. Three Dimensional Nano-Seeding Assembly of Ferromagnetic Fe/$LaSrFeO_4$ Nano-Hetero Dot Array. *J. Appl. Phys.* **2012**, *112*, 024320.
43. Yan, L.; Yang, Y.; Wang, Z.; Xing, Z.; Li, J.; Viehland, D. Review of Magnetoelectric Perovskite−Spinel Self-Assembled Nano-Composite Thin Films. *J. Mater. Sci.* **2009**, *44*, 5080–5094.
44. Comes, R.; Khokhlov, M.; Liu, H.; Lu, J.; Wolf, S. A. Magnetic Anisotropy in Composite $CoFe_2O_4$-$BiFeO_3$ Ultrathin Films Grown by Pulsed-Electron Deposition. *J. Appl. Phys.* **2012**, *111*, 07D914.
45. Aimon, N. M.; Kim, D. H.; Sun, X. Y.; Ross, C. A. Multiferroic Behavior of Templated $BiFeO_3$-$CoFe_2O_4$ Self-Assembled Nanocomposites, submitted **2014**.
46. Schneider, C. A.; Rasband, W. S.; Eliceiri, K. W. NIH Image to ImageJ: 25 Years of Image Analysis. *Nat. Methods* **2012**, *9*, 671–675.